



Prediction of femtosecond laser ablation profile on human teeth

Sarathkumar Loganathan¹ · Soundarapandian Santhanakrishnan¹ · Ravi Bathe² · Muthukumaraswamy Arunachalam³

Received: 22 May 2018 / Accepted: 17 September 2018 / Published online: 2 October 2018
© Springer-Verlag London Ltd., part of Springer Nature 2018

Abstract

To predict the laser ablation profile on dental hard tissue which will enable the user to optimize laser parameters so as to carry out the laser treatment with minimal tissue damage. The present study constructs a mathematical model to predict the ablation profile based on Gaussian beam distribution of laser intensity and correlates the model with experimentally obtained ablation parameters (effective Gaussian beam radius, ablation threshold fluence, and effective energy penetration depth). To obtain the ablation parameters, laser ablation experiments were carried out on dental hard tissues using Ti:Sapphire femtosecond laser (800 nm, 100 fs, 10 kHz). The method is further extended to predict the ablation rate and efficiency as well. The profile predicted from the mathematical model is compared with that of experimental results. It is found that the predicted ablation profile agrees well with the experimental profile for both enamel and dentin except a slight deviation at higher fluence for dentin. The calculated ablation rate is comparable to that of experimental results whereas for ablation efficiency appreciable deviation is observed in the case of dentin. The model succinctly predicts the ablation profile, ablation rate, and ablation efficiency which will enable to perform dental surgery at optimized laser processing conditions with high precision thus reducing the tissue damage appreciably. Once the details of lesion are known through proper diagnostic tools, the method enables the user to readily obtain optimum laser parameters. It can be used as a handy reference for dentists to perform damage-free surgery, ensuring quicker healing.

Keywords Ablation profile · Dental hard tissues · Femtosecond laser · Ablation threshold · Ablation rate · Ablation efficiency

Introduction

Tooth preparation is an essential part of dentistry. During tooth preparation, usage of conventional mechanical tools (hand instruments and high-speed air turbine) causes a lot of pain and discomfort to the patient, thus requiring local anesthesia [1]. In addition, mechanical drilling creates an unwanted reaction force, noise, and mechanical vibration which in turn reduce the accuracy and precision of surgery [2, 3].

Furthermore, direct contact between the diseased target tissue and mechanical instrument has a tendency of spreading a contamination layer on the healthy tissue leaving behind a large smear layer [4–6]. The smear layer may affect the bond strength of the restorative material which necessitates post-processing. Techniques such as etch-and-rinse mode and self-etch mode using phosphoric acid and universal adhesives can be employed for better bonding of restorative materials with dental hard tissues [7, 8].

In order to overcome the drawback of conventional drilling instruments, a laser-based non-invasive tooth preparation technique is introduced in dentistry using various conventional lasers typically of pulse duration ranging from continuous to nanosecond (ruby, CO₂, Er:YAG, ArF excimer laser, and Nd:YAG). However, undesired effects such as irreversible thermal damage of the pulp chamber, formation of carbonization layer at higher fluence, and low ablation rate are observed [2]. Ultrashort pulse laser (< picosecond) overcomes these issues by atomized material removal thus limiting the tissue damage with ablation rate ($0.44 \times 10^{-2} \text{ mm}^3/\text{s}$) higher than the rate of conventional laser but lesser than that of

✉ Soundarapandian Santhanakrishnan
sspandian@iitm.ac.in

¹ Manufacturing Engineering Section, Department of Mechanical Engineering, Indian Institute of Technology Madras,
<http://www.iitm.ac.in>

² Centre for Laser Processing of Materials, International Advanced Research Centre for Powder Metallurgy and New Materials (ARCI),
<http://www.arci.res.in>

³ Department of Periodontics, Tamilnadu Government Dental College,
<http://www.tamilnadudentalcollege.com>

conventional drilling instruments ($\sim 1 \text{ mm}^3/\text{s}$) [3, 9–11]. After several cavity preparation attempts, it is amply clear that ultrashort femtosecond laser (fs-laser) is the most promising non-invasive method suitable for removal of lesion from dental hard tissues (enamel and dentin) without undermining the safety [4, 9, 12, 13].

The fs-laser has high ablation efficiency compared to that of conventional laser. The thermal response and ablation dynamics of fs-laser differ completely from those of longer pulsed laser ($>$ picoseconds [14]). In fs-laser, energy of the photons absorbed by the electrons is transferred to phonons due to which ions are ejected in the form of ultrafast plasma from the target. Since the interaction time of fs-laser with target tissue is lesser than the thermal relaxation time (approximately from 100 ps to a few ns), maximum energy is carried away by ejected ions without any heat transfer to the adjacent tissues [3, 4, 15, 16]. As a result, fs-laser has the distinct advantage of reduced heat generation at the intrapulp region of the tooth, lower collateral damage, and higher ablation efficiency [5, 6, 9, 13, 17, 18].

Several studies [2–4, 12, 14, 19] have focused on investigating the influence of laser parameters on ablation characteristics of dental hard tissues. Niemz [3] investigated the ablation effect of Nd:YLF laser (30 ps, 1 kHz, and pulse energy up to 1 mJ) on sound and carious enamel surface. The study found that the ablation rate of carious enamel is higher than that of sound enamel. Chen et al. [2] developed a correlation between threshold fluence and laser beam waist radius and validated through experiments. The study reported that dentin exhibited maximum ablation efficiency of $0.020 \text{ mm}^3/\text{J}$ at the laser fluence of $6.51 \text{ J}/\text{cm}^2$ whereas enamel exhibited the same, $0.009 \text{ mm}^3/\text{J}$ at $7.59 \text{ J}/\text{cm}^2$. The effect of single pulse and multi-pulse on threshold fluence of enamel studied by Le et al. [12] reveals that the ablation threshold fluence decreases with increase in number of pulses. The results were reaffirmed by the studies of Nicolodelli et al. [4] in dentin and bovine femur bones. In addition, they observed increase in ablation diameter with increase in effective number of pulses which is contrary to Ji et al. [14] who observed increase in ablation depth without any change in ablation diameter. The complexity of laser ablation at the interface between bovine enamel and dentin was studied by Dutra-Correa et al. [19] and they proposed a method to predict the discontinuity of ablation diameter at the interface region of dental hard tissues using surface ablation data. Despite the studies of laser parameters on ablation depth and width, the complete ablation profile has not been explored on dental hard tissues.

Meanwhile, some of the researchers have also focused on developing numerical models for interaction of fs-pulsed laser with dental hard tissue by considering the two-temperature model (TTM) and classical Fourier series [20–24]. However, these models were unable to predict the teeth ablation dynamics and thermal response accurately due to the complex nature

of tooth's composite structure, tooth geometry, and unreliable dynamic thermophysical properties. Besides, they also require advanced computational resources and extensive simulation time [24]. Hence, there arises a need for a simple method to predict the ablation profile as a function of laser parameters which is essential to reduce the tissue damage on the tooth surface.

Therefore, this paper focuses on developing a reliable method to predict the laser ablation profile in enamel and dentin at a well-defined ablation region. An ablation profile function is derived, based on the spatial intensity distribution of fs-pulsed Gaussian laser beam. The developed ablation profile is validated with experimental results for both enamel and dentin irradiated by the fs-laser. This ablation profile prediction model can be effective on any lesion and dental hard tissues irrespective of age, race, and severity of the lesion.

Mathematical model for ablation profile and its correlation with ablation rate and ablation efficiency

The present work focuses on developing a correlation between ablation profile and ablation characteristics such as ablation rate and efficiency of fs-laser irradiated on dental hard tissues. The ablation profile is considered as a function of the spatial intensity distribution of the incident laser beam (Fig. 1). This, in turn, is expressed as a function of laser parameters such as effective Gaussian beam radius, ablation threshold fluence, and effective energy penetration depth within the well-ablated region of laser peak fluence (below $10.6 \text{ J}/\text{cm}^2$ for dentin and $24.7 \text{ J}/\text{cm}^2$ for enamel).

The Gaussian intensity distribution of laser fluence is expressed as follows [2, 25]

$$F(r) = F_p \cdot e^{-\frac{2r^2}{\omega_0^2}} \quad (1)$$

where r is the radial distance from the center of the beam spot, ω_0 is the focused beam waist radius on the surface of target, and F_p is the peak fluence at the center of the beam spot which is given by

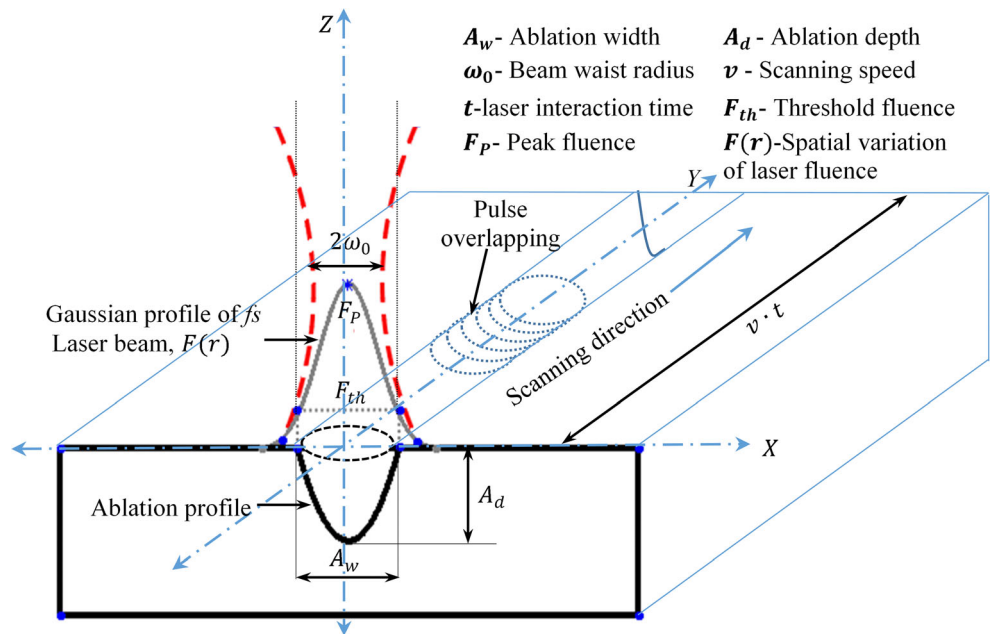
$$F_p = \frac{2E_p}{\pi\omega_0^2} \quad (2)$$

where E_p is the pulse energy in joules (J). The laser spot radius (r) is considered as the distance between the outermost point (x, y) and center of the beam spot (x_0, y_0) which is written as

$$r^2 = (x-x_0)^2 + (y-y_0)^2 \quad (3)$$

Substituting Eqs. (2) and (3) into Eq. (1), the laser fluence on the target surface is given by

Fig. 1 Schematic of laser-ablated groove and the spatial intensity distribution of laser beam



- A_w - Ablation width
- ω_0 - Beam waist radius
- t -laser interaction time
- F_p - Peak fluence
- A_d - Ablation depth
- v - Scanning speed
- F_{th} - Threshold fluence
- $F(r)$ -Spatial variation of laser fluence

$$F_{(x_0,y_0)}(x,y) = \frac{2E_p}{\pi\omega_0^2} \cdot e^{-\frac{2(x-x_0)^2}{\omega_0^2}} \cdot e^{-\frac{2(y-y_0)^2}{\omega_0^2}} \tag{4}$$

Considering the effective energy penetration depth (D_p) defined as $1/\alpha$ (where α is the absorptivity in cm^{-1}) along z -direction, the 3D Gaussian intensity distribution of the laser beam is given by

$$F_{(x_0,y_0,z_0)}(x,y,z) = \frac{2E_p}{\pi\omega_0^2} \cdot e^{-\frac{2(x-x_0)^2}{\omega_0^2}} \cdot e^{-\frac{2(y-y_0)^2}{\omega_0^2}} \cdot e^{-\frac{z-z_0}{D_p}} \tag{5}$$

Considering the power intensity distribution of scanning laser beam over xz -plane, the laser fluence profile can be written as

$$F_{(x_0,z_0)}(x,z) = F_p \cdot e^{-\frac{2(x-x_0)^2}{\omega_0^2}} \cdot e^{-\frac{z-z_0}{D_p}} \tag{6}$$

During the ablation process, the peak fluence (F_p) attains a critical value called ablation threshold (F_{th}) at which the material starts to vaporize from the surface of the target tissue at the focused beam spot. Hence, the ablation threshold (F_{th}) is expressed as

$$F_{(x_i,z_i)}(x,z) = F_p \cdot e^{-\frac{2(x_i-x_0)^2}{\omega_0^2}} \cdot e^{-\frac{z_i-z_0}{D_p}} = F_{th} \tag{7}$$

where (x_i,z_i) is the locus point at which the evaporation occurs in the enamel and dentin surface. Rearranging Eq. (7), the parabolic equation for the ablation profile is given by

$$\frac{2(x_i-x_0)^2}{\omega_0^2} + \frac{(z_i-z_0)}{D_p} = \ln\left(\frac{F_p}{F_{th}}\right) = \ln\left(\frac{E_p}{E_{th}}\right) \tag{8}$$

where E_{th} is the threshold pulse energy.

The ablation profile (Fig. 1) is obtained from the parabolic Eq. (8) once the ablation parameters such as F_p , ω_0 , D_p , and F_{th} are known. Here, (x_0,z_0) is considered to be an origin. Hence, $x_0 = z_0 = 0$. At maximum ablation depth, $x_i = 0$. Substituting this in Eq. (8), the maximum ablation depth (A_d) is given by

$$A_d = z_i = D_p \ln\left(\frac{F_p}{F_{th}}\right) \tag{9}$$

Therefore, Eq. (9) shows the linear relationship between ablation depth (A_d) and logarithmic of peak fluence (F_p). The values of D_p and F_{th} can be obtained from the slope and intercept of linear curve fit between A_d and $\ln(F_p)$ respectively.

Similarly, for maximum ablation width, $z_i = 0$. By substituting this in Eq. (8), the maximum ablation width (A_w) is obtained as

$$A_w = 2x_i = \sqrt{2} \cdot \omega_0 \cdot \sqrt{\ln\left(\frac{F_p}{F_{th}}\right)} \tag{10}$$

$$A_w^2 = 2\omega_0^2 \ln\left(\frac{F_p}{F_{th}}\right) = 2\omega_0^2 \ln\left(\frac{E_p}{E_{th}}\right) \tag{11}$$

From Eq. (11), the values of the effective Gaussian beam radius (ω_0) and threshold pulse energy (E_{th}) can be obtained from the slope and intercept of curve fitting between A_w^2 and $\ln(E_p)$. The predicted value of effective Gaussian beam radius from this method can be used to calculate peak fluence (F_p) given in Eq. (2). The threshold peak fluence (F_{th}) can be estimated using Eq. (11) as well.

By comparing both Eqs. (9) and (11), a correlation between the ablation depth and ablation width is obtained as Eq. (12) [25]

$$A_w = \omega_0 \sqrt{\frac{2A_d}{D_p}} \quad (12)$$

The present study has considered ablation rate (AR) as the volume of material removal per unit time (mm^3/s)

$$AR = A_{\text{area}} \cdot v \quad (13)$$

where A_{area} (mm^2) is the cross-sectional area of ablated groove in xz -plane and v (mm/s) is the laser scanning speed in y -direction. The cross-sectional area of ablated groove (A_{area}) is obtained by integrating Eq. (8) to the extent of maximum ablation width (A_w)

$$A_{\text{area}} = 2D_p \int_0^{A_w} \left[\ln\left(\frac{F_p}{F_{\text{th}}}\right) - \frac{2x^2}{\omega_0^2} \right] dx$$

$$A_{\text{area}} = D_p \cdot A_w \left[\ln\left(\frac{F_p}{F_{\text{th}}}\right) - \frac{A_w^2}{6\omega_0^2} \right] \quad (14)$$

Substituting Eq. (14) in Eq. (13), the ablation rate (AR) can be expressed as

$$AR = D_p \cdot v \cdot A_w \left[\ln\left(\frac{F_p}{F_{\text{th}}}\right) - \frac{A_w^2}{6\omega_0^2} \right] \quad (15)$$

The ablation efficiency AE (mm^3/J) is considered as the ratio between AR (mm^3/J) and average laser power P (W) and it is given by

$$AE = \frac{AR}{P} = \frac{D_p \cdot v \cdot A_w}{P} \left[\ln\left(\frac{F_p}{F_{\text{th}}}\right) - \frac{A_w^2}{6\omega_0^2} \right] \quad (16)$$

Experimental study

Sample preparation

Teeth freshly extracted due to periodontitis or orthodontic reasons were obtained from Tamil Nadu Government Dental College and Hospital, Chennai, India. The soft tissues were removed with curettes, washed in running distilled water, and preserved in formalin for 2 weeks. The top surface of the tooth was grounded in order to flatten out the surface of enamel but also care was taken to preserve the enamel surface by avoiding excess wear. The flat enamel surface was sectioned transversely to remove ~ 1.5 -mm-thick enamel layer using high-speed diamond disk. The samples were polished using silicon carbide (SiC) polishing paper (1200 grit size) with the presence of water as a coolant. Further, the samples were cleaned by

ultrasonication process with distilled water for around 3 min to remove any debris. The cleaned samples were stored in normal saline until the laser treatment so as to avoid dehydration. A similar procedure has been followed for the preparation of dentin samples as well.

Experimental method

The experiments were aimed at predicting the ablation profile in order to validate the mathematical model. Dental hard tissues (enamel and dentin) of thickness around 1–2 mm were irradiated by using the Spitfire Ace Power Amplifier Ti:Sapphire femtosecond laser. The laser system is capable of delivering the wavelength of 800 nm. The maximum average power of 12 W can be regulated using an ultrafast variable attenuator. Throughout the experiments, a lens with 50-mm focal length was used to focus Gaussian laser beam perpendicular to the sample surface with the help of automatic focusing CCD camera. The dental hard tissue of ~ 1.5 -mm thickness was loaded on high-precision CNC-controlled XYZ stage.

The grooves were produced on the surface of the tissue adopting single scanning line method of fs-laser at various processing conditions (Table 1). In order to ensure the repeatability, three trials were taken at each processing condition. The laser-irradiated samples were cleaned ultrasonically to remove any ablation debris and dried in air. The surface morphology of the fs-laser-ablated groove was measured by an optical profiler (Veeco NT-1100 profiler). The dimensions (depth and width) of the ablated groove were measured at three different regions of the scanning line.

Results and discussion

The proposed ablation profile function is given in Eq. (8) and depends on the laser ablation parameters such as effective Gaussian beam radius (ω_0), ablation threshold fluence (F_{th}), and effective energy penetration depth (D_p). In order to determine these ablation parameters, a single scanning line irradiation was carried out as a function of laser power at a constant scanning speed of 10 mm/s and 10-kHz repetition rate. The average power of laser was varied from 0.1 to 0.9 W for enamel and from 0.1 to 0.7 W for dentin so that the ablation profile could be obtained without any thermal damage.

The 3D profile of ablated grooves on the enamel surface at various power measured by optical profiler is illustrated in Fig. 2a. Figure 2a clearly indicates that the depth of ablation profile increases with the increase of power. The cross section of the ablation profile is found to be parabolic, as expected (Fig. 2b, c) at the power of 0.3 W and 0.7 W respectively. Similarly, the surface morphology of ablated dentin is also measured using the optical profiler.

Table 1 Laser processing conditions for 800-nm laser

Dental hard tissues	Average power ranging (W)	Scanning speed (mm/s)	Repetition rate (kHz)	Pulse duration (fs)
Enamel	0.1 to 0.9	10	10	100
Dentin	0.1 to 0.7	10	10	100

Determination of effective Gaussian beam radius (ω_0) and threshold fluence (F_{th})

In order to determine the effective Gaussian beam radius, the ablation width squared (A_w^2) is plotted against the pulse energy (in logarithmic scale) as shown in Fig. 2d. The curve fitting of experimental data for dentin and enamel is represented by dashed and solid lines respectively. According to Eq. (11), the slope of these fitted lines gives the value of $2\omega_0^2$ which enables to calculate the value of the effective Gaussian beam radius (ω_0) for dentin and enamel. The calculated value of ω_0 is found to be $(462.62/2)^{1/2} = 15.21 \mu\text{m}$ for enamel and $20.80 \mu\text{m}$ for dentin. The results indicate that the effective Gaussian beam radius of dentin is higher than that of enamel. In order to determine the threshold fluence values of enamel and dentin, the obtained effective Gaussian beam radius (ω_0) is used to evaluate the peak fluence at different laser pulse energies using the relation given in Eq. (2). The threshold fluence is

obtained experimentally by measuring the ablation width square and plotted against the logarithmic of peak fluence as in Eq. (11).

$$A_w^2 = 2\omega_0^2 \ln(F_p) - 2\omega_0^2 \ln(F_{th})$$

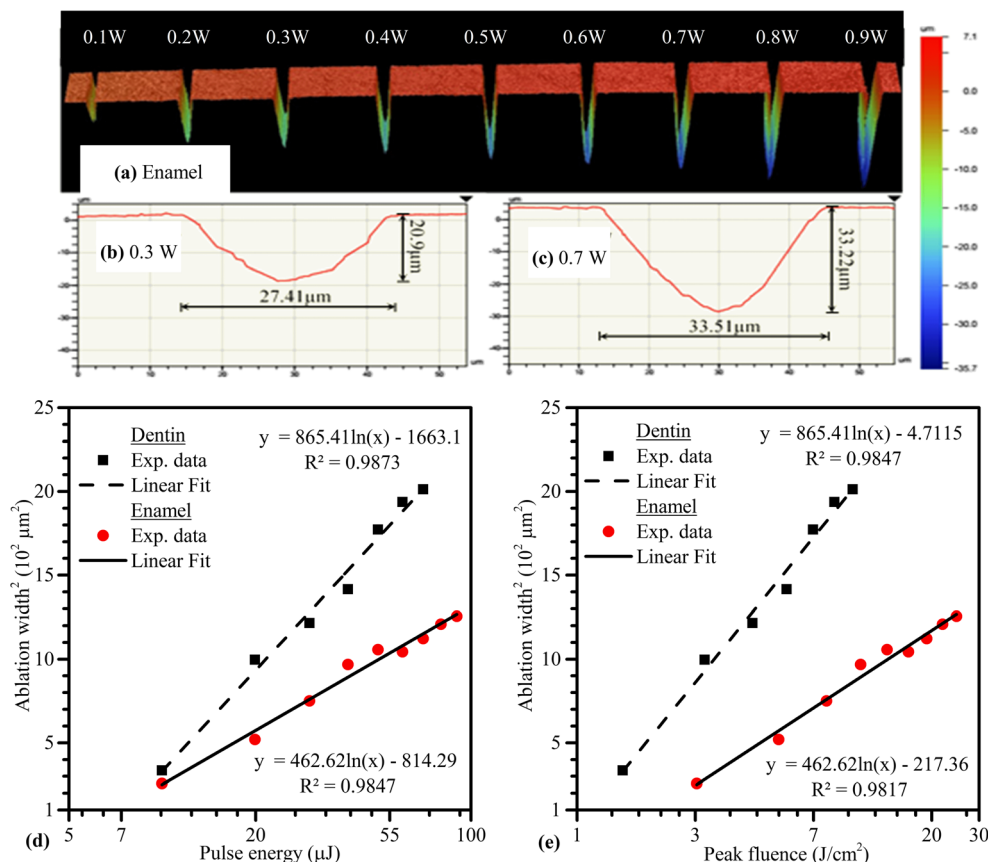
The slope will give the value of $2\omega_0^2$ whereas intercept is $2\omega_0^2 \ln(F_{th})$

$$\text{Intercept/slope} = 2\omega_0^2 \ln(F_{th}) / 2\omega_0^2 = \ln(F_{th})$$

$$F_{th} = \exp(\text{Intercept/slope}) \quad (17)$$

Figure 2e shows the plot between experimentally obtained values of ablation width squared versus peak fluence. The solid line and dashed line represent the curve fitting of experimental data of enamel and dentin respectively. The extracted value of threshold fluence according to Eq. (17) is found as $F_{th} = \exp(217.36/462.62) = 1.60 \text{ J/cm}^2$ for enamel and 1.01 J/cm^2 for dentin.

Fig. 2 a Optical 3D profile of the ablated grooves on the enamel surface (laser power varying from 0.1 to 0.9 W at the scanning velocity of 10 mm/s and repetition rate of 10 kHz). b Cross-sectional 2D profile of the groove at 0.3 W. c Cross-sectional 2D profile of the groove at 0.7 W. d Ablation width squared versus pulse energy (d) and peak fluence (e). Solid and dashed lines represent the curve fitting corresponding to the experimental data



The obtained threshold fluence for enamel is higher than that of dentin. This is mainly due to the microstructural arrangement and chemical composition of the dental hard tissues. The enamel is densely packed, highly mineralized, and more homogeneous with 85 vol.% of carbonated hydroxyapatite (CO₃-HAp). On the other hand, dentin is more porous and anisotropic with significant amount of organic material (collagen fibrils), water, and 47 vol.% of CO₃-HAp [11]. Since the threshold fluence of collagen fibrils (0.06 J/cm²) is less than that of hydroxyapatite (3.3 J/cm²), the dentin gets ablated at lower threshold fluence. The molecules of collagen fibril are covalently bonded with weak Vander Waal forces which leads to lower thermal stability than HAp [10]. In addition, the laser-induced breakdown of dentin tubule along the surface favors the enlargement of ablation diameter in dentin [14]. Thus, sufficient care must be taken upon ablating the dentin-enamel interface to avoid the incongruence of the ablated surface.

Determination of effective energy penetration depth (D_p) and effective number of pulses (N_{eff})

To determine the effective energy penetration depth of fs-laser on both dentin and enamel, the experimental ablation depth (A_d) is plotted against the peak fluence (in logarithmic scale) as shown in Fig. 3a. The curve fitting of experimental data for both dentin and enamel is represented with dashed and solid lines respectively. The fitted line equations are compared with the relation given in Eq. (9). According to Eq. (9), the slope of each fitted line is directly considered as the effective energy penetration depth (D_p) for the respective dental hard tissues. The value of D_p is found as 13.11 μm for enamel and 17.62 μm for dentin. The calculated results indicate that the effective energy penetration depth of dentin is higher than that of the enamel which might be attributed to the differences in absorption of the laser energy between the microstructures of enamel and dentin [19]. In addition, the intercept of the fitted line gives the threshold fluence which is found to be $F_{\text{th}} = \exp(6.01/13.11) = 1.58$ J/

cm² for enamel and 0.99 J/cm² for dentin. The values obtained from this ablation depth method are very close to the threshold fluence calculated from the ablation width square method in the “Determination of effective Gaussian beam radius (ω_0) and threshold fluence (F_{th})” section (i.e., 1.60 J/cm² for enamel and 1.01 J/cm² for dentin).

As the laser beam is scanning over the enamel and dentin surfaces at a constant line scanning speed, the effective number of pulses (N_{eff}) accumulated at each focused spot is a function of laser scanning speed (v), effective Gaussian beam radius (ω_0), and laser repetition rate (f) as [26]

$$N_{\text{eff}} = \sqrt{\frac{\pi}{2}} \cdot \frac{\omega_0 f}{v} \quad (18)$$

Since the effective Gaussian beam radius varies from material to material for the same waist radius of the laser beam, it is necessary to calculate the variation of effective number of pulses (N_{eff}) for different dental hard tissues.

According to Eq. (18), the effective number of pulses accumulated at each point on the center of the machined groove is found to be $N_{\text{eff}} = 19.06$ for enamel and 26.07 for dentin. Even though, the processing conditions of the laser are similar for both dentin and enamel, the difference in effective Gaussian beam radius leads to a difference in the effective number of pulses accumulated on both dental hard tissues. The ablation depth per pulse is approximately determined by dividing the experimentally obtained values of ablation depth (A_d) with the effective number of pulses. Figure 3b shows the plot between ablation depth per pulse and the peak fluence. As expected, the single pulse ablation depth increases with increasing peak fluence for both dental hard tissues.

Determination of ablation profile

The experimentally determined laser ablation parameters (ω_0 , F_{th} , D_p , N_{eff}) which is essential to predict the ablation profile of dental hard tissues are shown in Table 2. These parameters

Fig. 3 **a** Plot of the ablation depth as a function of peak fluence. **b** Ablation depth per pulse versus peak fluence. Solid and dashed lines represent the curve fitting corresponding to the experimental data

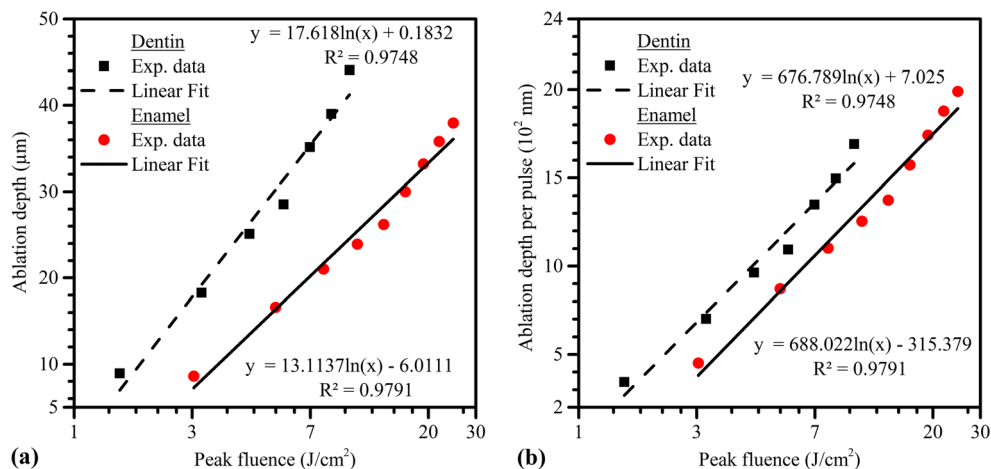


Table 2 Laser ablation parameters for dental hard tissues

Dental tissues	ω_0 (μm)	N_{eff}	D_p (μm)	F_{th} (J/cm^2)
Enamel	15.21	19.06	13.11	1.58
Dentin	20.80	26.07	17.62	0.99

are obtained using 100 fs, 800-nm Ti:Sapphire laser at a repetition rate of 10 kHz, and scanning speed of 10 mm/s.

The ablation parameters are initially validated based on the predictability of the width and depth. Figure 4a, b shows the variation of ablation width against the peak fluence for both dentin and enamel. Comparisons are made between the experimental (solid line) and calculated results (dashed line). The experimental results are in conformance with the calculated results. Similar comparisons are made for ablation depth as well. Thus, for the given parameters of ω_0 and D_p , if the ablation width is known, then the maximum ablation depth can be calculated and vice versa using Eq. (12).

Subsequently, the complete cross-sectional profile of the ablated groove is reconstructed by the parabolic Eq. (8) using the obtained laser ablation parameters. Figure 4c, d shows that the comparison of experimental and theoretical cross-sectional profile of groove lines for dentin and enamel surface respectively at different laser power (0.1 to 0.7 W for dentin and 0.1 to 0.9 W for enamel). These results clearly show that the ablation profiles are well matched at lower laser power (0.1 and 0.3 W) whereas the profile slightly deviates from the theoretical parabolic profile at higher laser power.

In addition, the increase of power from 0.3 to 0.7 W leading to only a moderate increase in the area of ablation profile indirectly indicates the decrease of ablation efficiency at higher power. This may be ascribed to the shielding effect at higher laser power [1]. Due to the homogeneous structure of enamel, the predicted ablation profile is in good agreement with experimental ablation profile as compared with that of dentin.

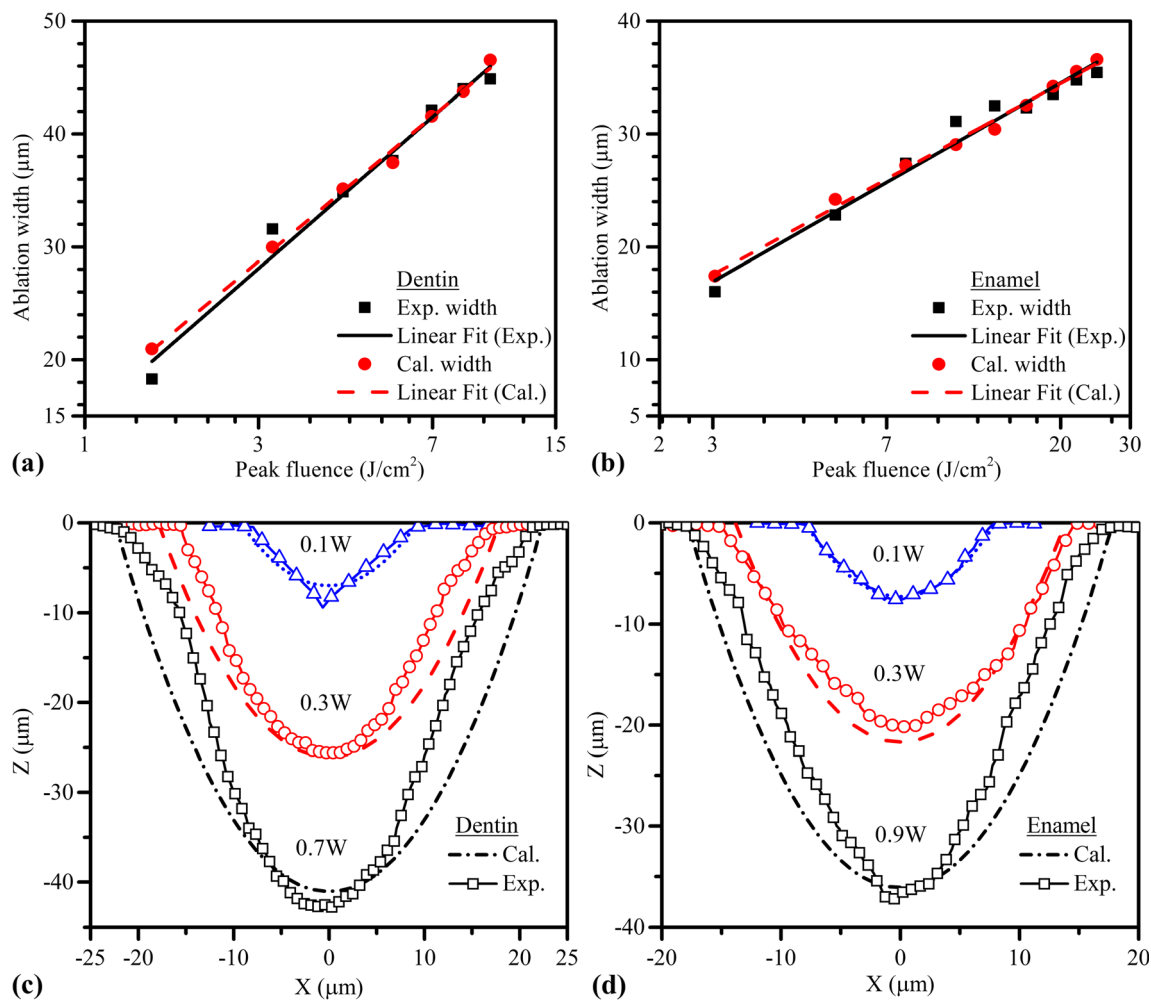


Fig. 4 Comparison between the experimental data and calculated results. Ablation width versus peak fluence for dentin (a) and enamel (b). The cross-sectional profile of ablated groove for dentin (c) and enamel (d) at different power

Role of peak fluence on ablation rate and ablation efficiency

The ablation profile obtained by the parabolic equation Eq. (8) can be further extended to calculate the ablation rate and ablation efficiency. Using the relation given by Eq. (15), the ablation rate can be approximately calculated once the ablation parameters (ω_0 , F_{th} , D_p , A_w) are known at various peak fluences (F_p) and scanning speed (v). Figure 5a shows the plot between the ablation rate and peak fluence for both dentin and enamel. The solid symbols denote the experimentally obtained ablation rate which is evaluated from the optical profiler data.

Figure 5a shows that the ablation rate increases with the peak fluence for both enamel and dentin but at a higher rate for dentin. However, at higher fluence, the ablation rate saturates for enamel. Such saturation is not apparent in dentin since the experiments were focused on the well-defined ablation region (average laser power < 0.7 W). The solid lines denote the ablation rate calculated using Eq. (15). The experimental and calculated ablation rate for enamel agrees well whereas for dentin, small deviation is noticed at higher laser fluence. This deviation is due to the deviation of ablation profiles in dentin which in turn might be due to its anisotropic and porous nature.

Similarly, the ablation efficiency is calculated using the relation given in Eq. (16) and compared with the experimental results in Fig. 5b. The ablation efficiency increases up to a certain limit of laser peak fluence (5.50 J/cm² for enamel and 4.41 J/cm² for dentin). It reduces gradually with further increase of fluence for both dentin and enamel. The experimental and calculated ablation efficiency as a function of peak fluence agrees well for enamel but shows an appreciable deviation for dentin. This deviation can be understood based on the large ablation profile deviation of dentin as observed in Fig. 4c.

In summary, the method is quite applicable for all ultrashort pulse laser of Gaussian beam profile, irrespective of lasing medium (Er or Nd or Er,Cr) and wavelength. The complex dynamics of laser-tissue interaction for various lasers is avoided by directly extracting the laser ablation from the experimental trials. However, for laser operating at longer pulse duration, the heat accumulation phenomena may reduce the well-defined ablation region which in turn reduce the precision of laser ablation parameters. In literature [2], it was reported that at higher laser fluence, the ablation of fs-laser produces undesirable effects like heat accumulation at the ablation zone which may lead to irreversible pulp damage, necrosis, and phase changes on target tissue. In order to avoid these effects, the laser should be operated at the optimized conditions. Despite operating at an optimized laser parameter, the target tissue should not undergo any structural phase change. In this study, no discernable phase change is observed which agrees with the earlier literature [3, 9, 11].

Since the thermophysical properties of dental tissues vary based on age, different teeth (incisor, canine, molar), different layers of each tooth (enamel and dentin), sex, race, and severity of the lesion, the interaction of laser with the dental hard tissues is hard to computationally model in real time (e.g., TTM and classical Fourier series). Moreover, the biological features like body fluids present in the dentin tubules and the heating-cooling effects of blood flow have to be considered in order to get a reliable prediction of ablation profile in the computational model [24]. Here, the complexity of the problem is avoided by employing a mathematical model which can easily predict the ablation profile of dental hard tissues at different peak fluences once the laser ablation parameters of the target are obtained from a few trial runs. Therefore, if the details of lesion (such as dimension of the lesion) are known through proper diagnostic tools (such as laser interferometry and fluorescence), the laser peak fluence can be

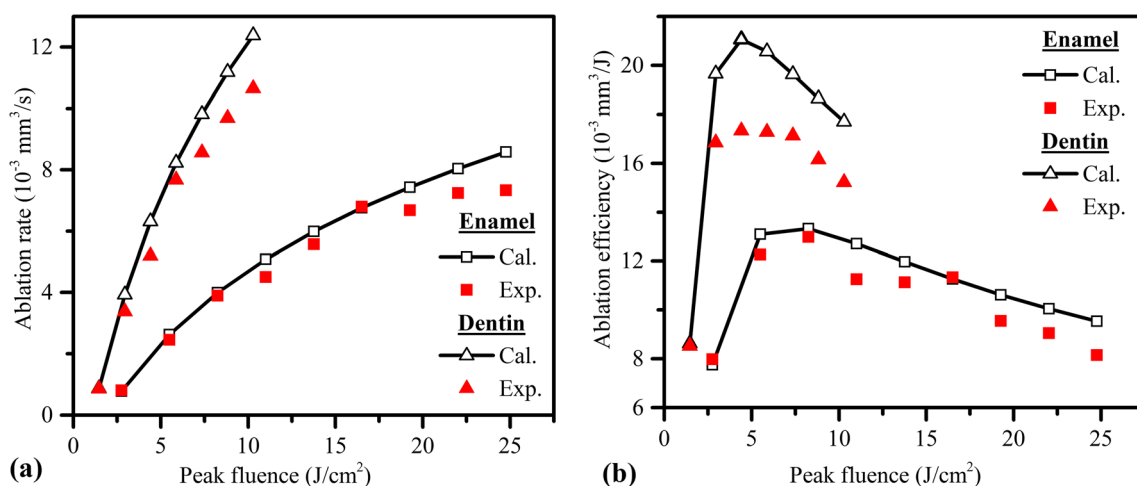


Fig. 5 Comparison between the experimental and calculated results. **a** Variation of ablation rate at different peak fluences for enamel and dentin. **b** Variation of ablation efficiency at different peak fluences for enamel and dentin

adjusted based on the extent of tissues which need to be removed. In addition, the method will also enable the user to optimize laser processing conditions so as to achieve maximum ablation rate and efficiency.

Conclusions

The mathematical model for laser ablation profile of dental hard tissues which is essential to avoid tissue damage was formulated based on Gaussian beam profile of laser beam. Femtosecond laser ablation was carried out on enamel and dentin in order to predict the ablation profile in terms of effective Gaussian beam radius, effective energy penetration depth, and ablation threshold fluence. A good correlation has been established between the calculated and experimental ablation profiles of microgrooves. In addition, the ablation rate and ablation efficiency are also calculated so as to obtain optimum laser parameters for dental treatment. This method can predict the ablation profile which will reduce the complexity of teeth ablation in different target tissues like various teeth, age, and severity of the lesion. The method will be applicable for all ultrashort pulse laser and it is very useful not only in dentistry but in orthopedic applications as well.

Compliance with ethical standards

Conflict of interest The authors declare that they have no conflicts of interest.

References

1. Shaheen ME, Gagnon JE, Fryer BJ (2014) Evaluation of ablation efficiency and surface morphology of human teeth upon irradiation with femtosecond laser pulses. *Laser Phys* 24:116001. <https://doi.org/10.1088/1054-660X/24/11/116001>
2. Chen H, Liu J, Li H et al (2015) Femtosecond laser ablation of dentin and enamel: relationship between laser fluence and ablation efficiency. *J Biomed Opt* 20:028004. <https://doi.org/10.1117/1.JBO.20.2.028004>
3. Niemz MH (1995) Cavity preparation with the Nd:YLF picosecond laser. *J Dent Res* 74:1194–1199. <https://doi.org/10.1177/00220345950740050801>
4. Nicolodelli G, de Fátima Zanirato Lizarelli R, Salvador Bagnato V (2012) Influence of effective number of pulses on the morphological structure of teeth and bovine femur after femtosecond laser ablation. *J Biomed Opt* 17:048001. <https://doi.org/10.1117/1.JBO.17.4.048001>
5. Kabas AS, Ersoy T, Gülsoy M, Akturk S (2013) Femtosecond laser etching of dental enamel for bracket bonding. *J Biomed Opt* 18:098003. <https://doi.org/10.1117/1.JBO.18.9.098003>
6. Liu J, Lü P, Sun Y, Wang Y (2015) Wettability of dentin after Yb : KYW thin-disk femtosecond ablation. *Lasers Med Sci* 30:1689–1693. <https://doi.org/10.1007/s10103-014-1655-8>
7. Stape THS, Wik P, Mutluay MM et al (2018) Selective dentin etching: a potential method to improve bonding effectiveness of universal adhesives. *J Mech Behav Biomed Mater* 86:14–22. <https://doi.org/10.1016/j.jmbm.2018.06.015>
8. Burke FT, Lawson A, Green DJ, Mackenzie L (2017) What's new in dentine bonding?: universal adhesives. *Dent Update* 44:328–340. <https://doi.org/10.12968/denu.2017.44.4.328>
9. Liu Y, Niemz M (2007) Ablation of femoral bone with femtosecond laser pulses - a feasibility study. *Lasers Med Sci* 22:171–174. <https://doi.org/10.1007/s10103-006-0424-8>
10. Le Q-T, Bertrand C, Vilar R (2016) Structural modifications induced in dentin by femtosecond laser. *J Biomed Opt* 21:125007. <https://doi.org/10.1117/1.JBO.21.12.125007>
11. Petrov T, Pecheva E, Walmsley AD, Dimov S (2018) Femtosecond laser ablation of dentin and enamel for fast and more precise dental cavity preparation. *Mater Sci Eng C* 90:433–438. <https://doi.org/10.1016/j.msec.2018.04.070>
12. Le Q-T, Bertrand C, Vilar R (2016) Femtosecond laser ablation of enamel. *J Biomed Opt* 21:065005. <https://doi.org/10.1117/1.JBO.21.6.065005>
13. Yuan F, Zheng J, Sun Y et al (2017) Regulation and measurement of the heat generated by automatic tooth preparation in a confined space. *Photomed Laser Surg* 35:332–337. <https://doi.org/10.1089/pho.2016.4242>
14. Ji L, Li L, Devlin H et al (2012) Ti: Sapphire femtosecond laser ablation of dental enamel, dentine, and cementum. *Lasers Med Sci* 27:197–204. <https://doi.org/10.1007/s10103-011-0932-z>
15. Verburg PC, Römer GRBE, Huis In'T Veld AJ (2014) Two-temperature model for pulsed-laser-induced subsurface modifications in Si. *Appl Phys A Mater Sci Process* 114:1135–1143. <https://doi.org/10.1007/s00339-013-7668-5>
16. Lin X, Zhang C, Ren W et al (2012) A theoretical model of the femtosecond laser ablation of semiconductors considering inverse bremsstrahlung absorption. *J Semicond* 33:046002. <https://doi.org/10.1088/1674-4926/33/4/046002>
17. Hoy CL, Ferhanoglu O, Yildirim M et al (2014) Clinical ultrafast laser surgery: recent advances and future directions. *IEEE J Sel Top Quantum Electron* 20:242–255. <https://doi.org/10.1109/JSTQE.2013.2287098>
18. Alves S, Oliveira V, Vilar R (2012) Femtosecond laser ablation of dentin. *J Phys D Appl Phys* 45:245401. <https://doi.org/10.1088/0022-3727/45/24/245401>
19. Dutra-Correa M, Nicolodelli G, Rodrigues JR et al (2011) Femtosecond laser ablation on dental hard tissues—analysis of ablated profile near an interface using local effective intensity. *Laser Phys* 21:965–971. <https://doi.org/10.1134/S1054660X11090064>
20. Chang KP, Tsai TW, Huang KY et al (2013) Thermal response of a dental tissue induced by femtosecond laser pulses. *Appl Opt* 52:6626–6635. <https://doi.org/10.1364/AO.52.006626>
21. Pike P, Parigger C, Splinter R, Lockhart P (2007) Temperature distribution in dental tissue after interaction with femtosecond laser pulses. *Appl Opt* 46:8374–8378. <https://doi.org/10.1364/AO.46.008374>
22. de Menezes RF, Harvey CM, de Martínez Gerbi MEM et al (2017) Fs-laser ablation of teeth is temperature limited and provides information about the ablated components. *J Biophotonics* 10:1292–1304. <https://doi.org/10.1002/jbio.201700042>
23. Letfullin RR, Rice CEW, George TF (2010) Bone tissue heating and ablation by short and ultrashort laser pulses. *Proc SPIE* 7548:75484K. <https://doi.org/10.1117/12.852455>
24. Lin M, Xu F, Lu TJ, Bai BF (2010) A review of heat transfer in human tooth-experimental characterization and mathematical modeling. *Dent Mater* 26:501–513. <https://doi.org/10.1016/j.dental.2010.02.009>
25. Cheng CW (2017) Ablation of copper by a scanning Gaussian beam of a femtosecond laser pulse. *Int J Adv Manuf Technol* 92:151–156. <https://doi.org/10.1007/s00170-017-0101-z>
26. Borowiec A, Haugen HK (2004) Femtosecond laser micromachining of grooves in indium phosphide. *Appl Phys A Mater Sci Process* 79:521–529. <https://doi.org/10.1007/s00339-003-2377-0>